Original Article

MOLECULAR METABOLISM

Targeted and selective knockout of the TLQP-21 neuropeptide unmasks its unique role in energy homeostasis

Bhavani S. Sahu [1,6,7], Maria Razzoli [1,7], Seth McGonigle [1,7], Jean Pierre Pallais [1], Megin E. Nguyen [1], Masato Sadahiro [2], Cheng Jiang [2], Wei-Jye Lin [2], Kevin A. Kelley [3], Pedro Rodriguez [1], Rachel Mansk [1], Cheryl Cero [1], Giada Caviola [4], Paola Palanza [4], Loredana Rao [5], Megan Beetch [1], Emilyn Alejandro [1], Yuk Y. Sham [1], Andrea Frontini [5], Stephen R. Salton [3], Alessandro Bartolomucci [1,*]

ABSTRACT

Objective: Pro-peptide precursors are processed into biologically active peptide hormones or neurotransmitters, each playing an essential role in physiology and disease. Genetic loss of function of a pro-peptide precursor results in the simultaneous ablation of all biologically-active peptides within that precursor, often leading to a composite phenotype that can be difficult to align with the loss of specific peptide components. Due to this biological constraint and technical limitations, mice carrying the selective ablation of individual peptides encoded by pro-peptide precursor genes, while leaving the other peptides unaffected, have remained largely unaddressed.

Methods: We developed and characterized a mouse model carrying the selective knockout of the TLQP-21 neuropeptide (ΔTLQP-21) encoded by the *Vgf* gene. To achieve this goal, we used a knowledge-based approach by mutating a codon in the *Vgf* sequence leading to the substitution of the C-terminal Arginine of TLQP-21, which is the pharmacophore as well as an essential cleavage site from its precursor, into Alanine ($R_{21} \rightarrow A$).

Results: We provide several independent validations of this mouse, including a novel in-gel digestion targeted mass spectrometry identification of the unnatural mutant sequence, exclusive to the mutant mouse. ΔTLQP-21 mice do not manifest gross behavioral and metabolic abnormalities and reproduce well, yet they have a unique metabolic phenotype characterized by an environmental temperature-dependent resistance to diet-induced obesity and activation of the brown adipose tissue.

Conclusions: The ΔTLQP-21 mouse line can be a valuable resource to conduct mechanistic studies on the necessary role of TLQP-21 in physiology and disease, while also serving as a platform to test the specificity of novel antibodies or immunoassays directed at TLQP-21. Our approach also has far-reaching implications by informing the development of knowledge-based genetic engineering approaches to generate selective loss of function of other peptides encoded by pro-hormones genes, leaving all other peptides within the pro-protein precursor intact and unmodified.

Keywords Pro-peptides; Mass spectrometry; Obesity; Point mutation; VGF; Granins

1. INTRODUCTION

Genetic loss of function is a powerful approach to identify the necessary role of gene products on cellular functions, physiology or diseases. While this approach is common for genes encoding a single protein product (receptors, structural proteins, signaling proteins, etc.), pro-peptide precursor genes pose a serious challenge because they encode multiple biologically-active peptides each having a different function and unique signaling [1—4]. Indeed, all the encoded peptides are simultaneously ablated using standard knockout approaches or cre-lox systems, resulting in a mixed phenotype which is difficult to explain from the loss of individual parts. Pro-peptides precursors such as pro-opio-melanocortin (POMC), pro-ghrelin, pro-glucagon, brain-derived neurotrophic factor, several granin peptides and many others, are key regulators of neuroendocrine functions and play essential roles in physiology and disease [1—4]. Notably, these peptides can be active on different receptors and exert very different biological functions. Classic examples include adrenocorticotropic

[1]Department of Integrative Biology and Physiology, University of Minnesota, Minneapolis, MN, 55455, USA [2]Nash Family Department of Neuroscience, Icahn School of Medicine at Mount Sinai, New York, NY, 10029, USA [3]Department of Cell, Developmental and Regenerative Biology, Icahn School of Medicine at Mount Sinai, New York, NY, 10029, USA [4]Department of Medicine and Surgery, University of Parma, 43120, Parma, Italy [5]Department of Life and Environmental Sciences, Universita' Politecnica delle Marche, Ancona, 60131, Italy

[6] Present address: National Brain Research Center, Manesar, 122052, India.
[7] These authors contributed equally to this work.

*Corresponding author. E-mail: abartolo@umn.edu (A. Bartolomucci).

Received April 26, 2023 • Revision received June 26, 2023 • Accepted July 18, 2023 • Available online 21 July 2023

https://doi.org/10.1016/j.molmet.2023.101781

hormone (ACTH), α−Melanocyte-stimulating hormone (αMSH) and β-endorphin, which are all derived by differential processing of the same POMC precursor [3]. Additionally, their tissue processing is tightly regulated by proteases leading to tissue-specific prevalence of only one or a few of those peptides. Lastly, to further complicate the biology of this system, some of these pro-peptide precursors also play a critical role in dense core granule biogenesis and stability [1,5,6]. Due to these biological constraints and technical limitations, mice carrying the selective ablation of only one peptide, encoded by a pro-peptide precursor gene leaving the other peptides unaffected, remains largely unaddressed. For example, while a knockout of the POMC precursor was developed long ago [7], there is no selective ACTH or β-endorphin knockout system that would also express the other unaltered POMC-derived peptides. One exception is a point mutant mouse in which a KKRR→QKQR mutation in the cleavage site of ACTH prevents the production of α-MSH [8]. In general, alternative approaches have been preferred, including the use of selective immune-neutralizing antibodies [2], and peptide injection into pro-peptide knockout mice [3]. These alternative approaches have limitations including specificity and bioavailability of the antibodies, and pharmacological properties of the drugs injected into knockout mice. Standard gene targeting approaches, CRISPR-Cas9, and other recent gene editing technologies, are all potentially useful approaches to address this limitation, each with different advantages and disadvantages [9].

The *Vgf* gene (non-acronymic) encodes for a 615 amino acid (617 in rodents) long pro-protein precursor of at least 8 biologically-active peptides [1]. VGF is cleaved by prohormone convertases (PC)1/3 and PC2 to generate low molecular weight peptides which are secreted through the regulated pathway [1,10]. Thus - much like for POMC - germline [11,12], or tissue-specific [6,13,14] VGF null mice, or humanized knock in mice in which the human *VGF* coding sequence replaces the mouse coding sequence in the mouse *Vgf* gene locus [15], are not informative about the biology of any individual VGF-encoded peptides. Additionally, the physiology of VGF is also complicated by the structural role of the pro peptide which is likely relevant for dense-core granule biogenesis and secretion of other peptides by endocrine cells (e.g. insulin in beta-cells) [1,6]. Among the VGF-derived peptides, the C-terminal internal 21 amino acid long fragment known as TLQP-21 [16], is arguably the most studied and best characterized; also being the only one for which a clear receptor-mediated mechanism has been identified thus far [17−19]. First identified in the rodent brain [16], and later in sympathetic and sensory nerves [20,21] and in endocrine glands such as the adrenal medulla [22], TLQP-21 emerged as a pleiotropic neuropeptide involved in various physiological processes such as lipolysis, microglial activation, pain, sexual behavior and energy balance [1,17]. However, most of our knowledge on TLQP-21 derives from pharmacological gain of function experiments, while selective loss of function approaches have not been attempted yet. Here, after reconstructing the evolutionary history of TLQP-21 highlighting a strong selective pressure on its pharmacophore in mammals, we generated and initially characterized a TLQP-21-selective knockout mouse (aka, ΔTLQP-21). We took advantage of previous knowledge demonstrating that the C-terminal Arginine, which is necessary for TLQP-21 biological activity [17,19,23], is also required for cleavage from its precursor TLQP-62 [10,20,24]. We mutated the codon in the *Vgf* sequence encoding for the C-terminal Arginine into a codon encoding Alanine (R_{21}→A) which results in the production of a peptide sequence that is not a substrate for pro-hormone convertase [25]. This resulted in a mouse lacking TLQP-21 while showing normal expression of pro-VGF and the TLQP-21 precursor TLQP-62. ΔTLQP-21 mice do not have gross behavioral and metabolic abnormalities, yet they manifest an unexpected metabolic phenotype characterized by an environmental temperature-dependent resistance to diet-induced obesity.

2. RESULTS

2.1. The evolutionary history of the TLQP-21 neuropeptide suggests that an intense selective pressure occurred at its C-terminus in mammals

Recent evidence suggests that C3a/TLQP-21/C3aR1 genes underwent intense selective pressure in mammals [23]. Specifically, while C3a was identified as the ancestral ligand of C3aR1 based on sequence analysis and is highly conserved across mammals [23], TLQP-21 pharmacophore and C3aR1 binding pocket were subject to mutation during evolution which conferred a gain of function in the *Murinae* subfamily of rodents [23].

We have now expanded our evolutionary analysis on TLQP-21 (and also included C3a and C3aR1) including 161 mammalian sequences found in NCBI and focused on the C-terminal amino acid motif Proline-Proline-Alanine-Arginine (-$PPAR_{21}$), the essential amino acids required for receptor binding and activation [19], with the R_{21} also representing a recognition site for prohormone convertase to cleave TLQP-21 from its precursor TLQP-62 [1] and for putative plasma proteases to deactivate the peptide [1,19,23,24]. We found that R_{21} is highly conserved (68% of species) and that the amino acid Serine (S) prevails at position 20 in mammals including humans, and can thus be considered the ancestral sequence ([23] and Supplementary Table 1). Conversely, A_{20} is unique to *Murinae/Cricetinae* (Figure 1 A,B and Supplementary Table 1). Interestingly, there are only 2 exceptions to the $S/A_{20}R_{21}$ motif (Figure 1C): i) marine mammal species (Artiodactyla: Balaenopteridae, Delphinidae, Monodontidae, Phocoenidae, Physeteridae) invariably express S_{21}; ii) 38 species including carnivores (Canidae, Felix, Mustelidae), ursidae and horses express histidine (H) at position 21 (Supplementary Table 1). Neither H or S are canonical consensus sites for pro-hormone convertase [25], thus suggesting that TLQP-21 might not be produced in these species. This evolutionary sequence analysis indicates that selective pressures acted in different species on amino acids critical for TLQP-21/C3aR1 receptor recognition, while the C-terminus of C3a remains largely conserved across mammals (Figure 1). Yet, the functional significance of those mutations remains largely unknown. Here we aimed to shed light on this question by generating a mouse model in which TLQP-21 cannot be cleaved from its precursor TLQP-62.

2.2. Generation and characterization of ΔTLQP-21 mice

TLQP-21 is a C-terminal internal fragment, which can only be produced upon cleavage of the precursor TLQP-62 [16]. By utilizing gene targeting constructs previously employed to generate the VGF knockout mice [11] and inserting flanking loxP sites into the mouse Vgf locus [26], we introduced a mutation in the VGF coding sequence ($P_{573}PAR_{576}$ ccacctgcgcgc to $P_{573}PAA_{576}$ ccacctgcggcg) leading to R_{21}→A mutation (Figure 2A). Sanger sequencing confirmed the correct mutation in the ΔTLQP-21 mutated mouse (Figure 2B). Staining the hypothalamus (Figure 2C) and the adrenal gland (Supplementary Figure. 1A) of WT and ΔTLQP-21 mice with a selective rabbit-anti-mouse TLQP-21 antibody [20] confirmed the loss of TLQP-21 in ΔTLQP-21 animals. This mutation is predicted to result in the inability of pro-hormone convertases to cleave the peptide from TLQP-62 [16]. To verify that this mutation did not impact the pro-peptide processing

A

C3a

motif	All	Primates	Rodentia	Muridae	Cricetidae	Artiodactyla	Delphinidae
LAR	142	25	34	9	12	27	5
LGT	27	6	0	0	0	10	0
Others	7	0	0	0	0	0	1
Total	176	31	34	9	12	37	6

C3aR

motif	All	Primates	Rodentia	Muridae	Cricetidae	Artiodactyla	Delphinidae
DHV*	110	28	2	0	0	27	5
DNV*	8	0	5	0	0	0	0
DHM	9	0	9	7	2	0	0
DHL*	6	1	0	0	0	0	0
DCV*	4	0	4	0	0	0	0
Others	35	1	11	2	6	0	0
Total	172	30	31	9	8	27	5

VGF

motif	All	Primates	Rodentia	Muridae	Cricetidae	Artiodactyla	Delphinidae
PSR	67	23	15	0	0	7	0
PAR	22	0	22	11	11	0	0
PSH	36	0	0	0	0	0	0
Others	36	0	0	0	0	14	4
Total	161	23	37	11	11	21	4

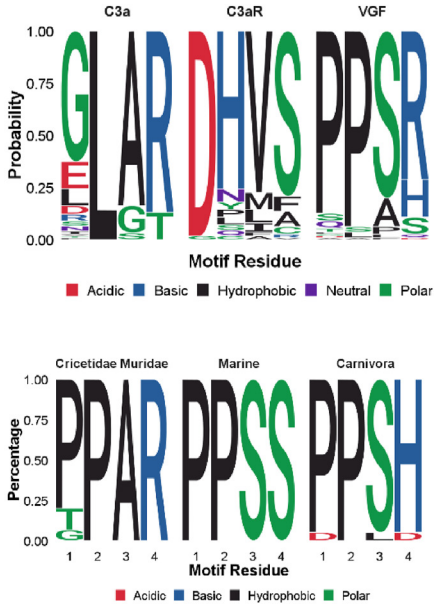

Figure 1: Evolutionary analysis of C-terminal TLQP-21 sequence. A) Table of C-terminal C3a and TLQP-21 and selected residues in the C3aR1 binding pocket motifs from NCBI Protein RefSeq database. **B)** Sequence logos of mammals for C3a C terminus, C3aR1 binding pocket and TLQP-21 pharmacophore. **C)** Sequence logos of mammals for the last 4 amino acids of TLQP-21 in selected groups of mammals. See Supplementary Table 1 for a complete sequence list.

in general, we blotted brain extracts using a C-terminal antibody which recognizes the VGF pro-peptide and all precursor fragments containing the C-terminus, including TLQP-62 [27]. Results show an identical profile of VGF fragments in WT and ΔTLQP-21 mice in the hypothalamus (Figure 2D). This result suggests that preventing the cleavage of TLQP-21 does not impact the pro-peptide nor does it increase the accumulation of its precursor TLQP-62. Lastly, expression of *Vgf*, *C3aR1* and *C3* in several key organs was unaffected by the ΔTLQP-21 mutation (Supplementary Figure. 1B).

To confirm the $R_{21} \rightarrow A$ mutation at the protein level we developed a novel in-gel digestion-based mass spectrometry (MS) analysis for TLQP-21 using an approach similar to what was used for other peptides [28] (Figure 3A). Fresh adrenal gland was rapidly lysed in RIPA lysis buffer and equal amounts of proteins were loaded in a 12% precast gel and were resolved in the MES buffer system along with the synthetic TLQP-21 peptide. Gels were stained with Safe blue followed by excision of bands between ~2KD to ~5KD corresponding to a region where TLQP-21 would be identified based on its molecular weight (MW) [16]. Excised bands followed tryptic digestion and were analyzed by targeted MS. The point mutation $R_{21} \rightarrow A$ in the VGF coding sequence results in the loss of a prohormone processing site leading to new peptide fragment transitions predicted by the Skylab software, such as AQAR and HFHHALPPAAHHPDLEAQAR (Figure 3B). Our MS analysis reveals that those predicted fragments can only be detected in the ΔTLQP-21 mice while being absent in the WT (Figure 3C,D; Supplementary Figure. 2), overall validating the mouse model at the protein level.

2.3. ΔTLQP-21 mice show normal development and behavior

TLQP-21 has been implicated in multiple biological functions [1,16,17,29,30], thus we conducted a thorough characterization of ΔTLQP-21 mouse behavior and physiology. ΔTLQP-21 mice are viable, and homozygous or heterozygous mice can reproduce with a similar success rates and manifest similar maternal behavior (Supplementary Tables 2–3). Male and female ΔTLQP-21 mice from homozygous or heterozygous breeding pairs reached comparable weight at weaning suggesting similar developmental rates (Supplementary Table 4). Due to the known effects of pharmacological treatment with TLQP-21 on behavior [14,31,32], mice were also tested in traditional behavioral assays to detect anxiety-like and depression-like traits, but again, no differences were found compared to WT (Supplementary Figure. 3). Based on a similar phenotype we opted to continue the experiments using pups from heterozygous pairs, allowing for better control of the early maternal environment, and using littermates for all the following experiments.

2.4. ΔTLQP-21 mice are resistant to diet-induced obesity at room temperature

One of the best-characterized functions of TLQP-21 is to potentiate adrenergic-induced lipolysis [20,23,33]. Consistently, plasma free glycerol measured in response to 3 h cold challenge at 4 °C was decreased in ΔTLQP-21 male and female mice (Supplementary Figure. 4A). Conversely, free glycerol induced by a β-adrenergic receptor (β3AR) agonist, which does not activate sympathetic transmission and thus TLQP-21 secretion from neurons, was unaffected by TLQP-21 deletion (Supplementary Figure. 4B).

Based on the catabolic role exerted by TLQP-21 upon central or peripheral administration [16,33,34], we initially hypothesized that its selective deletion might result in obesity. At two months of age, male and female ΔTLQP-21 and WT mice were singly housed and monitored for their body weight growth and food intake in response to standard diet and standard housing temperature of 21 ± 1 °C. No differences emerged for body weight, food intake, body composition, energy expenditure, insulin tolerance, glucose tolerance, and fasting glucose due to the mouse genotype (Supplementary Figures. 5 and 6), suggesting that deletion of TLQP-21 does not affect energy or glucose homeostasis, under standard housing conditions.

Next, we challenged the ΔTLQP-21 mice with an obesogenic high fat diet (HFD). Contrary to our hypothesis, and similar to VGF−/− and C3aR1−/− mice [11,35], both male and female ΔTLQP-21 mice were

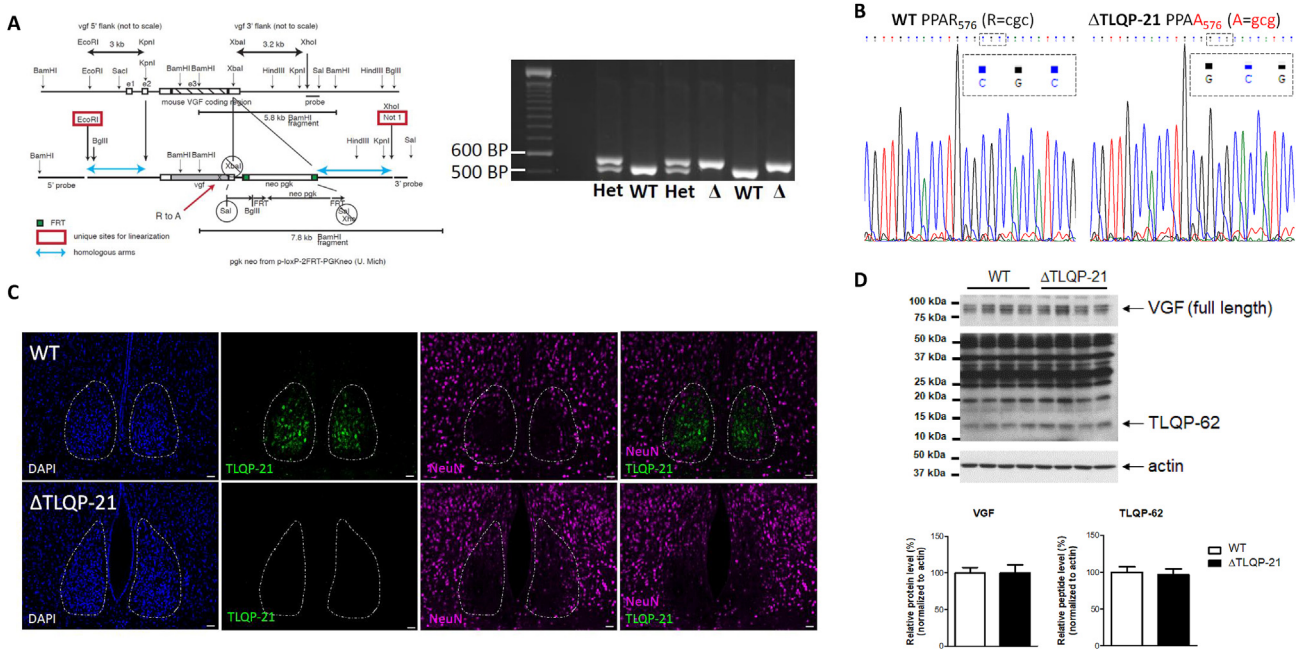

Figure 2: Generation and characterization of ΔTLQP-21 mice. A) Schematic for the generation of ΔTLQP-21 mice and PCR amplification. Specific primers were designed to amplify the genomic ΔTLQP-21 region of the *Vgf* gene, followed by gel extraction of the purified product, which reveals a single specific ~180 base pair amplicon of this VGF region. **B)** Sanger sequencing. The TLQP-21 PCR amplified region was gel purified and subjected to Sanger sequencing. The results were analyzed using Chromas Lite software, and base changes in the ΔTLQP-21 mice were confirmed by manually inspecting the peaks of the chromatogram. **C).** IHC of the hypothalamus. The suprachiasmatic nucleus (SCN) shows a particularly strong TLQP-21 staining, and is included as the representative area of positive staining. As expected based on previous studies [27], SCN neurons express little NeuN antigen. The brain was stained with antibodies for TLQP-21 or NeuN. Images representative of N = 4. **D).** Western blotting of the hypothalamus. A VGF C-terminal specific primary antibody was used to detect on the same blot with different exposure lengths, the VGF pro-protein (top panel, 75—100 kDa), and the TLQP-21 precursor TLQP-62 (middle panel, 10—15 kDa), along with a number of additional C-terminal-containing VGF-derived peptides (middle panel, 15—50 kDa). The actin loading control was visualized in the lower panel (37—50 kDa). Relative levels of VGF and TLQP-62 normalized to actin, for WT and ΔTLQP-21 samples (WT = 100%) were analyzed by Student's t-test (ns, N = 4).

resistant to diet induced obesity as demonstrated by significantly lower body weight gain and fat mass gain (Figure 4 A-D) without showing a distinct food intake, or fat free mass gain compared to WT (Supplementary Figure. 6). Consistent with the leaner phenotype, plasma insulin was significantly lower, and insulin sensitivity was higher in ΔTLQP-21 mice than WT (Figure 4E—H). Unexpectedly, resistance to obesity was not paralleled by improved glucose tolerance or fasting glucose levels (Supplementary Figure. 6). Since improved insulin tolerance emerged only in ΔTLQP-21 mice fed a HFD only, in association with lower insulin level, our results suggest that improved glucose homeostasis is secondary to a leaner phenotype, and not primarily attributed to altered insulin secretion [36,37].

The brown adipose tissue (BAT) of ΔTLQP-21 male mice fed HFD appeared markedly more activated, with brown adipocytes having smaller lipid droplets and higher level of UCP1 compared to WT (Figure 5A,B). Consistent with the morphological analysis, the BAT of male ΔTLQP-21 mice fed HFD showed increased *Ucp1, Cox71a, Zic1, and Adrb3* expression, while no differences emerged in mice fed a standard diet (STD) (Figure 5C). Morphologically, the perigonadal white adipose tissue (pWAT) but not the subcutaneous inguinal (sc)WAT of male mice fed HFD visually showed a higher proportion of smaller-size adipocytes in ΔTLQP-21 mice, which is consistent with obesity resistance (Supplementary Figure. 6I). Also, adipocytes in the pWAT and scWAT were uniformly unilocular, suggesting minimal (if any) beiging. Consistent with this observation, UCP1 mRNA was only sporadically detected in the scWAT of male mice fed HFD (1/6 WT, 2/6 ΔTLQP-21), and other thermogenic/beiging gene markers were also highly variable, with a significant increase observed only for *Cidea* (Supplementary Figure. 6K). Fat pad morphology and gene expression of female ΔTLQP-21 was substantially similar to the one of female WT mice, with a prominent effect of HFD. The BAT of female mice had a more activated appearance than in males consisting of smaller adipocytes and high levels of *UCP1*, and effect which was more evident in ΔTLQP-21 mice (Figure 5; Supplementary Figure. 6J). In females as well, adipocytes in the pWAT and scWAT were uniformly unilocular (Supplementary Figure. 6J), *UCP1* mRNA was only sporadically detected in the scWAT (0/6 WT, 2/6 ΔTLQP-21), and no significant increase was observed in other thermogenic/beiging gene markers (Supplementary Figure. 6L).

The resistance to HFD-induced obesity and the BAT morphology in ΔTLQP-21 mice housed at room temperature (22 ± 1 °C), suggest increased energy expenditure. However, heat production measured via indirect calorimetry at the end of the study was not increased in either males or females (Figure 4 I—P).

2.5. The obesity resistance of ΔTLQP-21 mice depends on adaptive thermogenesis requirements

Based on the unexpected resistance to diet-induced obesity, and considering the previously established role for TLQP-21 in energy balance, we tested the hypothesis that the metabolic phenotype was caused by a compensatory response to sub-thermoneutral housing at room temperature which is known to drive sympathetic tone and norepinephrine/β-adrenergic receptor (NE/βAR) signaling to metabolic organs in order to sustain body temperature and metabolism [38—40]. To test this hypothesis, we housed ΔTLQP-21 and WT mice at 28—

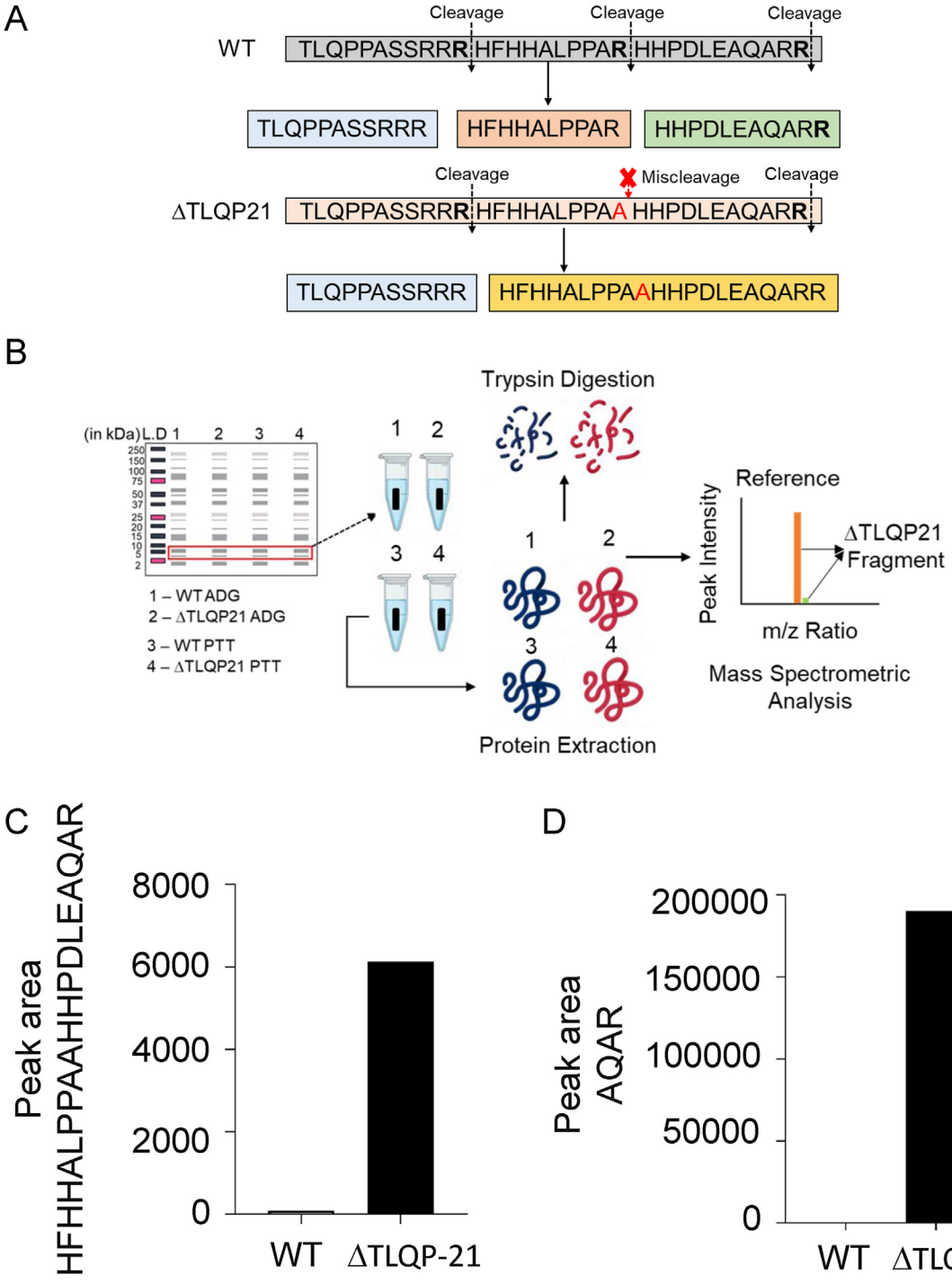

Figure 3: Targeted mass spectrometry. A). A targeted mass spectrometry-based approach was used to characterize the misprocessing of TLQP-21 in ΔTLQP-21 mice. Tissue samples were subjected to gel electrophoresis along with the synthetic TLQP-21 peptide followed by excision, tryptic digestion, and analysis by targeted mass spectrometry. **B)**. Schematic of WT and ΔTLQP-21 sequences showing predicted cleavage sites and the point mutation R→A. **C,D)**. Targeted mass spectrometry of the adrenal gland. The R→A mutation in the ΔTLQP-21 mice ablated a proteolytic processing site which resulted in a larger tryptic fragment HFHHALPPAAHHPDLEAQAR and the presence of AQAR which is normally not present in TLQP-21. Representative MS spectra of WT and ΔTLQP-21 are shown in Supplementary Fig. 2.

30 °C, a temperature selected to minimize adaptive thermogenic demands. Supporting our hypothesis, this housing condition was sufficient to prevent resistance to HFD-induced obesity in ΔTLQP-21 mice as evidenced by body weight, food intake, body composition and glucose homeostasis, all of which resulted in non-significant differences from WT mice (Figure 6). In addition, no significant differences were found for energy expenditure, fat-free mass, and food intake (Figure 6; Supplementary Figure. 7). Interestingly, while some of the thermogenic genes were normalized by these housing conditions, *Ucp1* and *Cox71a* were still significantly elevated in ΔTLQP-21 mice (Figure 6I).

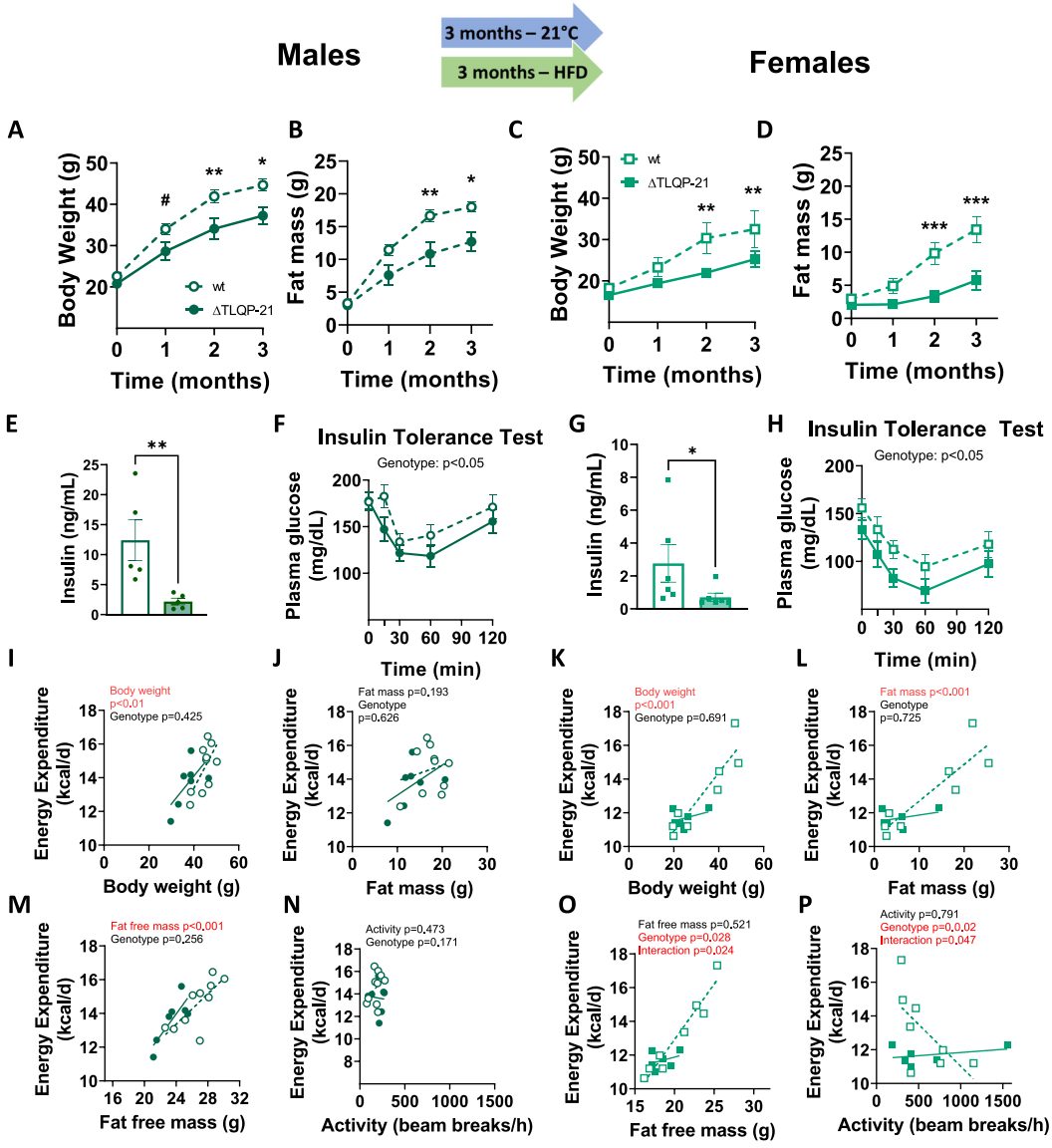

Figure 4: Metabolic phenotypes of ΔTLQP-21 mutant male and female mice and their wild type counterparts tested at room temperature (21 ± 2C°) and ad libitum fed 60% High Fat Diet (HFD). (A-B,C-D) Both male and female ΔTLQP-21 mice gained significantly less body weight (main effect genotype: $F(1,32) = 11.12$, $p < 0.01$; main effect sex: $F(1,32) = 39.86$, $p < 0.0001$; main effect time on diet: $F(3,96) = 139.74$, $p < 0.0001$) as well as fat mass (main effect genotype: $F(1,32) = 13.75$, $p < 0.001$; main effect sex: $F(1,32) = 20.00$, $p < 0.0001$; main effect time on diet: $F(3,96) = 85.35$, $p < 0.0001$) over time than WT mice. (E–H) ΔTLQP-21 mutant mice of both genders showed a significantly lower non fasting insulin (Male: $U = 0$; Female: $U = 4$; note that data were not normally distribute d and were analyzed with the non-parametric Mann Whitney U Test) and greater insulin sensitivity (main effect genotype: $F(1,34) = 5.04$, $p < 0.05$; main effect sex: $F(1,34) = 20.71$, $p < 0.0001$) than WT animals. (Area under the curve (mg*min/dL): WT Male = 18.8 ± 1.4, ΔTLQP-21 Male = 16.7 ± 1.0, WT Female = 13.5 ± 1.5, ΔTLQP-21 Female = 10.5 ± 1.0). Energy expenditure over 24 h was significantly influenced by body mass in both males and females (I,K), by fat mass in females (L) and by fat free mass in males (M). In female mice, genotype significantly influenced energy expenditure that was lower in ΔTLQP-21 mice, while interacting with both fat free mass (O) and activity (P). N = 6–9/group. Data in A-D and F,H were analyzed with repeated measure ANOVA with time point and genotype as main factors; symbols indicate differences between genotypes at each time point. # represents $1 > p > 0.05$; * represents $p < 0.05$; ** represents $p < 0.01$. Data in I–P were analyzed using ANCOVAs with the factor indicated on the x axis as continuous predictor.

2.6. Investigating the role of sympathetic innervation in the phenotype of ΔTLQP-21 mice

The environmental temperature-reversible resistance to dietary challenge manifested by the ΔTLQP-21 mice, is paradoxical when considering the effect exerted by exogenous TLQP-21 treatment [16,33,34], yet it is consistent with the obesity resistance manifested by VGF−/− mice [12,12,15], overall suggesting that TLQP-21 deletion causes a compensatory increase of sympathetic drive to the BAT.

ΔTLQP-21 male and female mice (housed at room temperature and fed a STD) showed a significantly higher temperature response to acute cold challenge, and in response to the pharmacological challenge with the β3AR agonist CL316243 than wild type (Supplementary Figures. 4C and D), suggesting that the resistance to HFD-induced obesity could be driven by the sympathetic nervous system. However, HFD fed ΔTLQP-21 mice housed at room temperature (i.e. the group showing the maximal metabolic effect), showed normal density of TH-positive sympathetic fibers, TH abundance assessed by WB, and

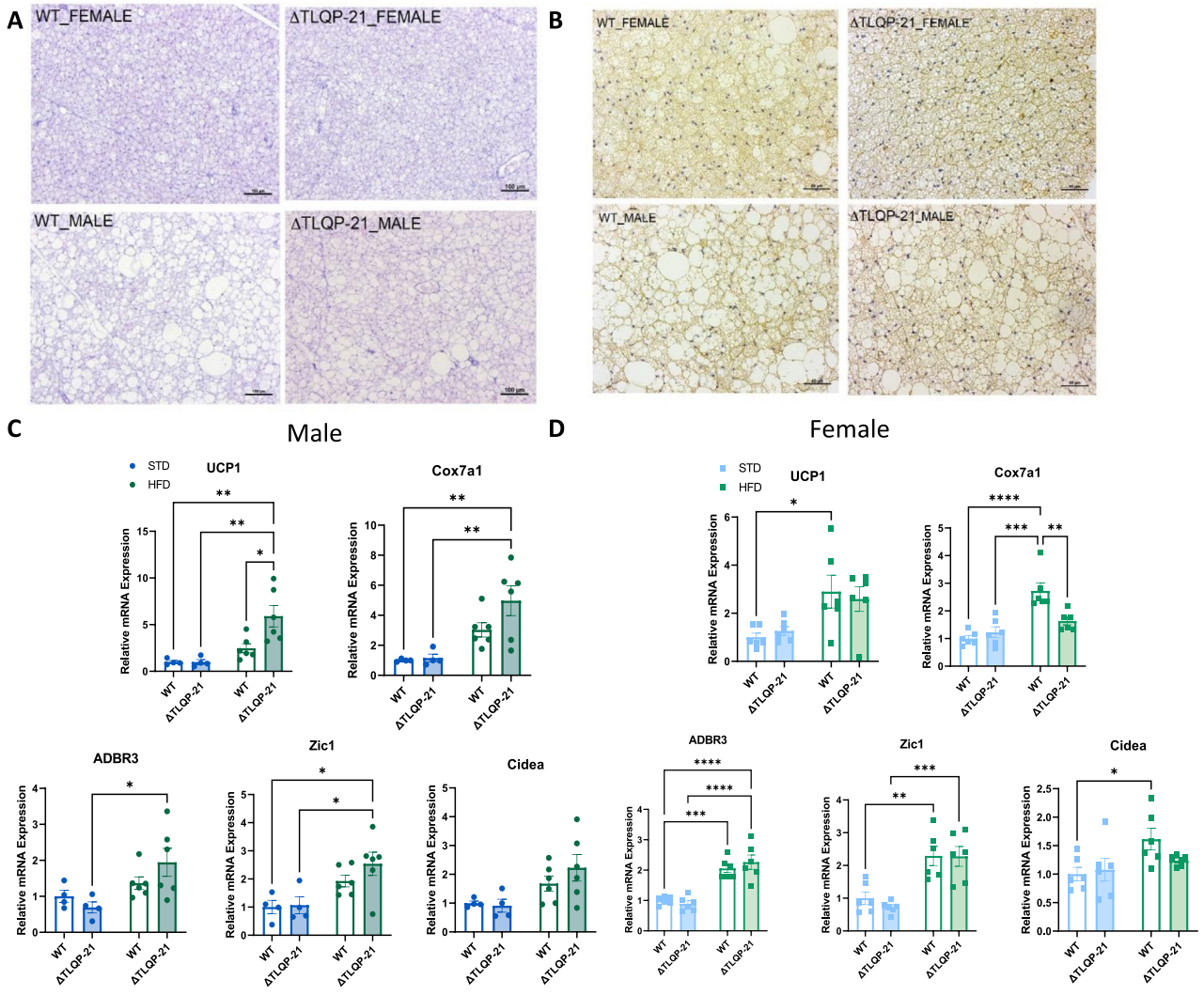

Figure 5: Brown adipose tissue morphological and molecular analysis. A) H and E staining and **B)** IHC for UCP1 in BAT obtained from male (bottom row) and female (top row) in WT and ΔTLQP-21 mice housed at RT and fed with HFD. **C,D**). QPCR of genes implicated in brown adipocyte thermogenesis and browning in WT and ΔTLQP-21 male and female fed standard diet (STD) or a high fat diet (HFD) and housed at room temperature. UCP1 (Males: genotype F (1,16) = 4.737, p = 0.0448, diet F (1,16) = 16.34, p = 0.0009, interaction F (1,16) = 4.764, p = 0.0443; Female: diet F (1,20) = 13.14, p = 0.0017), Cox7a1 (Male: genotype F (1,20) = 4.892, p = 0.0388, diet F (1,20) = 30.05, p < 0.0001; interaction F (1,20) = 11.46, p = 0.0029; Females: diet: F (1,16) = 17.76, p = 0.0007), ADRB3 (Males: diet F (1,16) = 8.298, p = 0.0109; females: diet F (1,20) = 69.05, p < 0.0001), Zic1 (Males: diet F (1,16) = 13.48, p = 0.0021; females: diet: F (1,20) = 37.61, p < 0.0001), Cidea (Males diet: F (1,16) = 8.387, p = 0.0105; females: diet: F (1,20) = 6.580, p = 0.0185). Data in C,D were analyzed with two-way ANOVA with diet and genotype as main factors with Tukey's multiple comparisons test as ad hoc analysis. Symbols represent individual ΔΔCt values normalized over WT at STD. * represents p < 0.05, ** represents p < 0.01, *** represents p < 0.001, and **** represents p < 0.0001.

NE abundance in the BAT (or the scWAT) (Supplementary Figures. 8A–C). Overall, these results suggest that acute sympathetically-drive thermogenic response is increased in the ΔTLQP-21 mice, yet this phenotype is not responsible for the resistance to HFD induced obesity, highlighting the complexity of the phenotype caused by the selective deletion of TLQP-21.

3. DISCUSSION

Here we developed and initially characterized a mouse model carrying the selective loss of the VGF-derived TLQP-21 peptide leaving expression of the VGF pro-protein or its processing, intact. Additionally, we showed that preventing the cleavage of TLQP-21 does not significantly increase the accumulation of its direct precursor TLQP-62 [16], a result that can be ascribed to the rapid proteolytic cleavage of small peptides [24,29]. The generation of the ΔTLQP-21 mouse was achieved by generating a knock-in mouse carrying a selective point mutation in the codon encoding for R_{21} that is required for its proteolytic cleavage (and is also required for its biological activity via C3aR1 activation [1,16,17]). Validation of this model included: i) Sanger sequencing of the gene; ii) a novel in-gel digestion targeted proteomics which allowed unambiguous confirmation of the model by identifying a non-natural fragment (HFHHALPPA**A**HHPDLEAQAR) created by the $R_{21} \rightarrow A$ mutation; iii) absence of immunoreactivity to a selective anti-TLQP-21 antibody in the adrenals and hypothalamus [20,30].

Despite previous work suggesting a role for TLQP-21 in sexual behavior and reproduction [41–43], ΔTLQP-21 mice reproduce well and perform normal maternal behavior. Additionally, when mice are

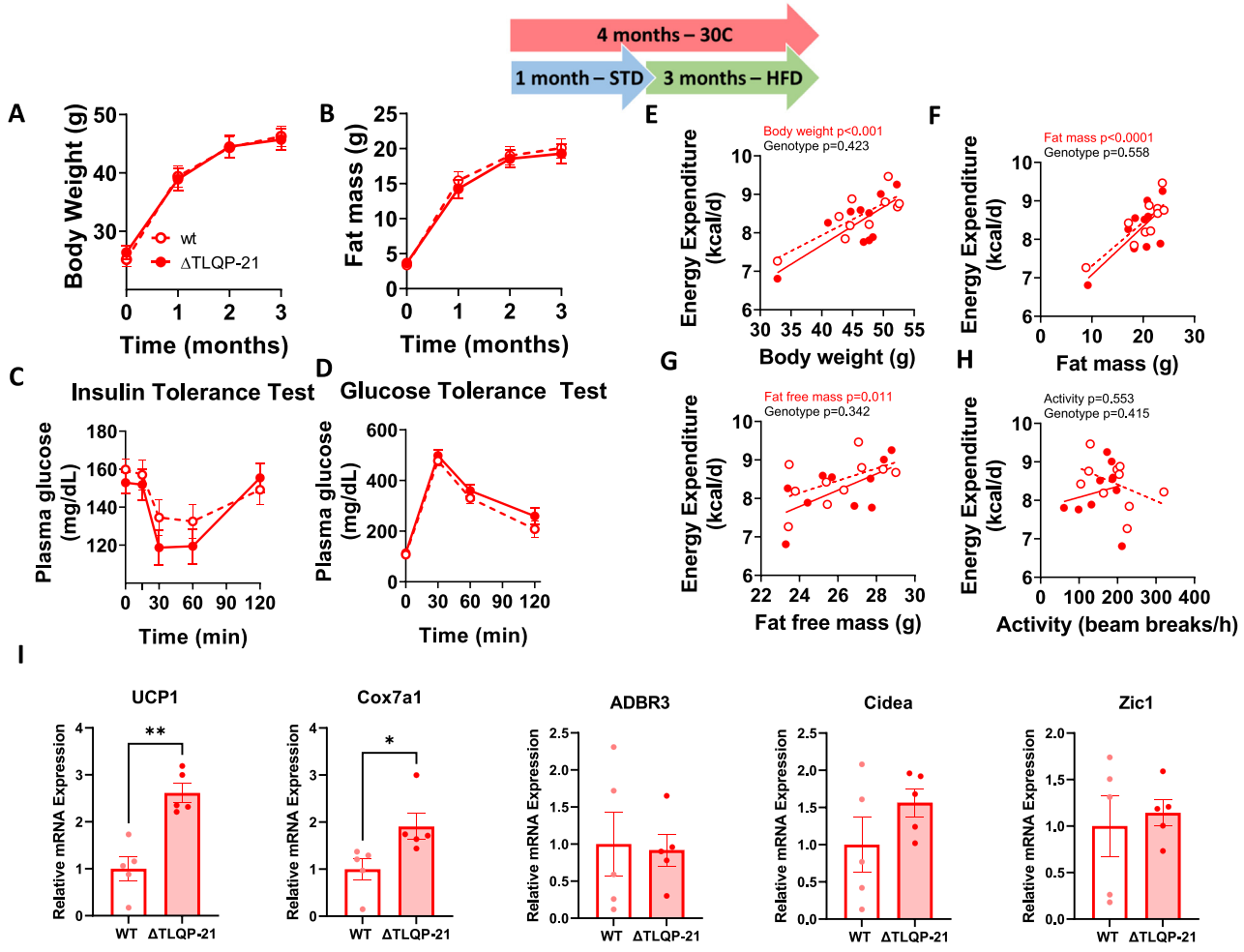

Figure 6: Metabolic phenotypes of male ΔTLQP-21 mutant and wild type mice tested at 30 ± 1°C and ad libitum fed a 60% High Fat Diet (HFD). ΔTLQP-21 mice did not differ from WT mice in either body weight or fat mass gain over time (A,B), nor in insulin tolerance (Area under the curve (mg*min/dL): WT = 17.0 ± 1.0, ΔTLQP-21 = 16.1 ± 0.5) or glucose tolerance (Area under the curve (mg*min/dL): WT = 37.0 ± 2.0, ΔTLQP-21 = 40.6 ± 2.6) tests (C,D). Energy expenditure assessed during the course of 24 h showed no dependency on genotype but a significant dependency on mouse body weight (E), fat mass (F), and fat free mass (G), with no relationship to activity levels (H). N = 10/group. (I) QPCR of genes implicated in brown adipocyte thermogenesis and browning. UCP1 ($p = 0.0010$), Cox7a1 ($p = 0.0343$). Data were analyzed using two-tailed unpaired t-test. Symbols represent individual ΔΔCt values and normalized to WT. * represents $p < 0.05$, ** represents $p < 0.01$.

fed a standard diet, the R21A mutation does not confer gross behavioral or metabolic abnormalities except for a defective acute cold-induced lipolysis, which is consistent with a role for TLQP-21 to potentiate adrenergic induced lipolysis *in vitro* and in vivo [20,23,24,33]. ΔTLQP-21 mice manifest increased insulin tolerance on HFD. The pro-VGF protein is important for regulating insulin granules formation [[6]], a function likely unaltered in the ΔTLQP-21 mice since the pro-peptide is unaffected (Figure 2). Additionally, both TLQP-62 and TLQP-21 are insulinotropic peptides (TLQP-62 > TLQP-21 [[37]]). TLQP-62 is unaffected in the ΔTLQP-21 mice. Also, ΔTLQP-21 mice show improved insulin tolerance (and lower insulin level), and normal glucose tolerance, only under HFD but not STD. These observations led us to conclude that the improved sensitivity is likely secondary to the leaner phenotype manifested by the ΔTLQP-21 mice rather than a direct effect of the mutation on insulin secretion.

Based on the anti-obesity effect exerted by central/peripheral TLQP-21 injection or VGF over-expression in mice or hamsters [16,33,34,44], we initially hypothesized that ΔTLQP-21 mice would be vulnerable to HFD-induced obesity. Contrarily to our hypothesis, ΔTLQP-21 mice were resistant to HFD-induced obesity, a phenotype that cannot be explained by changes in food intake, activity or, surprisingly, energy expenditure, which were all unaffected by the ablation of TLQP-21. It is possible that technical limitations in the use of indirect calorimetry [45,46] prevented the detection of increased energy expenditure and/or that energy compensation mechanisms were activated [47–49]. Two lines of evidence suggest this conclusion. Firstly, the BAT (but not the scWAT) of ΔTLQP-21 mice showed increased markers of activation when compared to WT, suggesting increased thermogenic capacity. Secondly, minimizing adaptive thermogenesis requirements by housing mice at 28–30 °C prevented the obesity resistant phenotype from manifesting. It is thus possible that selective germline deletion of TLQP-21 caused a compensatory augmentation of other thermogenic pathways overall resulting in a paradoxical resistance to obesity despite a catabolic role for the peptide itself. While this hypothesis requires additional experimental support to be mechanistically understood, two lines of evidence seems to indirectly support it. First, we detailed the existence of a strong selective pressure in mammals on the C-terminus of TLQP-21 (see [23] and Figure 1). We showed that

the $S_{20}\rightarrow A$ mutation is exclusive to *Murinae* and *Cricetinae* and conferred a gain of function resulting in enhanced potency at the C3aR1 receptor to regulate lipolysis [23]. We speculate that selective pressures favored the emergence of a pro-lipolytic and thermogenic mechanism in small-sized rodents. In the absence of this mechanism, due to genetic loss of function, one of two outcomes would be possible: i) ablating the peptide could result in hypothermia and/or defective lipolysis and obesity; ii) due to its physiological relevance, the genome/phenome could respond by activating and/or increasing the efficacy of other catabolic pathways. That the second scenario can be correct is suggested by the consistent (thus far considered paradoxical) resistance to obesity manifested by other models including VGF−/− [11,12], the C3aR−/− [35], a CNS-selective VGF knockout [26] as well as a humanized mouse carrying a selective truncation of a large portion of the VGF C-terminus including TLQP-21 [15]. It is thus possible that lack of TLQP-21 may be the main reason why VGF−/− mice or the other models discussed above were resilient to HFD-induced obesity [11,12,26]. Furthermore, a humanized knock in mouse carrying a full length human VGF, including the S_{20} at the C-terminus of TLQP-21, is prone to obesity [15]. Overall, these results suggest that the ancestral $-SR_{21}$ sequence [23] which is shared with humans can cause the pro-obesogenic phenotype in mice which was predicated based on the catabolic effect of pharmacological treatment of WT mice/adipocytes with TLQP-21 [20,33]. Conversely, the absence of TLQP-21 in the germline of ΔTLQP-21 and in the VGF−/− mouse models, could trigger the activation of compensatory physiological mechanisms leading to the obesity resistant phenotype. One such compensatory mechanism could be increased adaptive thermogenesis mediated by the BAT/scWAT [50]. However, while ΔTLQP-21 manifest increased thermogenic response to cold or β3AR challenge, BAT TH and NE are normal and there are only modest changes in beiging markers in the scWAT. Several mechanisms mediating adaptive thermogenesis independent from the canonical sympathetic-noradrenaline-βARs pathway leading to UCP-1 mediated uncoupling [51,52], have recently been identified [50,53–59], thus future studies should be focused on identifying the mechanism of the resistance to HFD induced obesity cause by TLQP-21 deletion.

4. LIMITATIONS AND FUTURE DIRECTIONS

This study also has some limitations. Due to the complex biology of VGF and TLQP-21, and technical challenges with the generation of organ specific or conditional R21A mutants, we cannot rule out a developmental role for the TLQP-21 peptide in metabolic tissues, such that TLQP-21 ablation in the germline (of either the ΔTLQP-21 or the VGF−/− [11]) results in altered BAT morphology and activity, and resistance to HFD-induced obesity, while peptide administration in the adult animal generally has the opposite effect. Additionally, although i) proteolytic processing of pro-VGF is unaffected by the R576A mutation, ii) no biologically active peptide generated by proteolytic cleavage of TLQP-21 has been identified thus far, and iii) ΔTLQP-21 mice have normal behavior and physiology (except when challenged with HFD or environmental thermogenic demands), we cannot exclude that the mutation could result in the accumulation of unknown biologically active peptide fragments. Further studies should clarify this aspect. Finally, this experiment adhered to recommended standards in metabolic studies by testing young adult mice fed a STD, or a HFD for 12 weeks [60]. Yet, we cannot exclude that a longer diet duration on HFD or aging could affect the metabolic phenotype of the ΔTLQP-21 mice differently from what reported in the present study.

5. CONCLUSION AND FUTURE PERSPECTIVES

Here we developed a mouse model of selective loss of TLQP-21. The ΔTLQP-21 line can be a valuable resource to conduct mechanistic studies on the necessary role of TLQP-21 in physiology and disease, while also serving as a platform to test the specificity of novel antibodies or immunoassays directed at TLQP-21. We focused our characterization on energy balance, metabolism and behavior, which revealed a unique role for this peptide in response to dietary and environmental challenges. We did not test other biological roles attributed to TLQP-21 such as in nociception, gastrointestinal function, blood pressure, and others. Thus, additional work is necessary to characterize the physiology of this mouse model in full.

Aside from testing specific hypotheses relevant to VGF and TLQP-21 biology, our approach can have far-reaching implications by informing the development of similar knowledge-based genetic engineering approaches to generate selective loss of function of other peptides encoded by pro-hormones genes, leaving all other peptides within the pro-protein precursor intact and unmodified. These studies can open new vistas to further characterize the biology of many biologically active peptide hormones encoded by pro-peptides whose function has been studied thus far using mostly gain of function or complete loss of function gene ablation approaches.

6. METHODS

6.1. Generation of Vgf ΔTLQP21 mouse line

The floxed VGF ΔTLQP21 ($R_{21}\rightarrow A$) knockin mouse line was generated by inserting a 5′ flanking loxP site into the Vgf 5′ UTR (KpnI site), and a 3′ flanking loxP site and FRT-flanked neomycin selection cassette, derived from p-loxP-2FRT-PGKneo (Dr. David Gordon, University of Colorado Health Science Center), into the Vgf 3' UTR (XbaI site), using previously described mouse Vgf genomic sequences [11]. This previously described VGF construct [27] underwent targeted mutagenesis (Mutagenex Inc., Hillsborough NJ) to introduce a mutation encoding a TLQP-R21A amino acid substitution ($mVGF_{1\text{-}617}$ R576A). The plasmid sequence was verified and the targeting construct was electroporated into 129Sv/J-derived R1 embryonic stem (ES) cells by the Mouse Genetics and Gene Targeting Core Facility, Icahn School of Medicine at Mount Sinai, as described previously [11,61]. Southern and PCR analyses confirmed correct gene targeting. Male chimeras were mated with C57BL/6J females to produce F1 breeders and experiments were performed on N2F1 mice.

6.2. Genotyping and Sanger sequencing

Genomic DNA was isolated from the mouse tails using the Qiagen DNA extraction kit. The VGF region of interest was PCR amplified with specific primers VGF-P.11-for 5′-TCACCCCTTCCCAAACTACA-3′ and VGF-P.11-rev 5′- ATTCTCCAGCTCCTCCTGCTC-3′, and the resultant amplicon was gel purified. Gel-purified amplicons were subjected to Sanger sequencing by using the same primers. The results were analyzed using Chromas Lite software, and base changes in the ΔTLQP-21 mice were confirmed by manually inspecting the peaks of the chromatogram. The TLQP-21 region of the Vgf gene was PCR amplified and sequenced at the University of Minnesota Genomics Center. Chromatograms were manually analyzed using Chromas Lite software for the mutations, and the peaks were extracted for the same.

6.3. Mass spectrometry

For mass spectrometry, fresh tissues (3 adrenal glands) for WT and ΔTLQP-21 were collected and lysed in lysis buffer (2.5% SDS,

100 mM Tris, pH 8) using a bead-based homogenizer. Lysates were cleared; the BCA method was used to estimate protein (Thermo Fisher). Equal amounts of protein were loaded in each well and resolved on 12% gels (Invitrogen, Bolt) with MES buffer. A molecular weight marker ladder (Dual Extra Plus, Bio-Rad) was used. In parallel, the synthetic peptide was also loaded for precise gel excision of the TLQP-21 region. Gels were resolved at 200 V for 30 min, washed with HPLC grade water and stained using safe blue stain (Invitrogen) for 60 min, followed by de-staining using HPLC grade water. With the synthetic peptide and the molecular weight marker as a reference, gel bands were excised using sterile scalpels and stored at −20° until further processing. In-gel digestion was carried out per standard protocols, and the tryptic peptides were used for further analysis. Peptide MS Analysis: peptide digestions were dried and solubilized in 20ul of 2% acetonitrile, 98% water and 0.1% formic acid. 2ul was loaded on an Eksigent 2.7uM HALO fused-core c18 column (100 mm × 0.3 mm) using an Agilent 1100 series microflow pump. The peptides were loaded on the column at a rate of 8ul/min for 2 min and a linear gradient from 2% acetonitrile (ACN) to 45% ACN for 17.5 min. The ACN was then increased to 90% for 2 min and then to 2% ACN for 5 min. The Applied Biosystems 5500 ion trap was used using a turbo V electrospray source fitted with a 25uM ESI electrode. Transitions and parameters predicted from an insilico tryptic digestion of the synthetic TLQP-21 peptide with all partially digested fragments considered. The tryptic-digested synthetic peptide validated the MS parameters determined using the Skyline program [62]. The data was analyzed using MultiQuant™ (ABI Sciex, Framingham, MA, USA), which provides the peak areas for the transitions.

6.4. General in vivo procedures

Experimental mice were maintained in a fully controlled animal facility (12:12 h light:dark cycle at 22 ± 1 °C, unless otherwise specified). Heterozygous breeding pairs were established and pups were weaned in groups of same-sex siblings. Animal experiments were conducted at the University of Minnesota (USA) and approved by the Institutional Animal Care and Use Committee, University of Minnesota. Mice were fed a standard (D12450B, Research Diets 3.85 kcal/g, 10% kcal from fat) or a high fat (D12492, Research Diets, 5.24 kcal/g, 60% kcal from fat, HFD) diet.

Mice undergoing experiments at thermoneutrality, were transferred from the vivarium to an adjacent fully controlled environmental room and housed in a 12:12 h light:dark cycle at 30 ± 1 °C. Mice were allowed one month to acclimate to 30 ± 1 °C before performing any experimental procedure.

In separate studies, ΔTLQP-21 and WT male and female mice (n = 8–10/group) were single housed and assessed for: body weight, food intake, body composition, glucose homeostasis, energy expenditure and behavior, cold and β-adrenergic receptor sensitivity. The study design also incorporated environmental factors such as housing temperature (standard housing temperature 22 °C or mouse thermoneutral temperature 28–30 °C) and diet (standard diet or high fat diet). Body weight and food intake were measured regularly during the experiments.

6.5. Maternal behavior

Maternal behavior was assessed by observing ΔTLQP-21 (n = 6), WT (n = 5) and heterozygous (n = 7) mothers in their home cages, from post-natal day (PND) 1 to 14. Dams behavior was analyzed in the last 2 h of the light cycle by the same operator who was unaware of the mouse genotype. Each lactating female was observed once every 4 min, for a total amount of 30 observations in 2 h for each dam. During each 4 min observation, the experimenter recorded the behavior displayed at the moment of the observation. Dams behaviors were identified according to standard behavioral categories [63] including: arched back (AB) nursing, nursing, licking, nest building, grooming, active. We also calculated the time spent out of the nest; considering all the observations during which the dam was anywhere in the cage but the nest, regardless of the behavior exhibited at the moment of the observation. In addiction we put together all behaviors related to pups (AB, nursing, nest building, licking pups) and we compared it with total of behaviors not related to pups (out of nest, active, grooming).

6.6. 4 h fasting glucose, glucose tolerance test, insulin tolerance test

Fasting glucose was measured 4 h following food removal by tail bleeding. Glucose tolerance test was performed following an overnight fast. Blood glucose levels from tail bleeding were monitored at 0, 30 60 and 120 min after an i. p. injection of D-glucose at 2 g/kg. Insulin tolerance test was performed following a 6 h fasting period. Mice were injected i. p. with a dose of 0.75 IU/kg of insulin and blood glucose levels were monitored at 0, 15, 30, 60, and 120 min after injection. Glucose was measured with Accu-chek Aviva glucometers (Roche Diagnostics, Indianapolis, IN).

6.7. Indirect calorimetry and body composition

Oxygen consumption (VO_2), carbon dioxide production (VCO_2), Heat, Respiratory Efficiency Ratio (RER) and activity were measured using the Oxymax Comprehensive Lab Animal Monitoring System (Columbus Instruments, Columbus, OH). Energy expenditure was calculated with the formula provided by the manufacturer, expressed as kcal/h and analyzed with body weight, fat mass, fat free mass or activity as continuous predictor in an ANCOVA model. Body composition was measured with EchoMRI 3-in-1 (EchoMRI LLC, Houston, TX). Variables were measured in a rapid (approximately 70 s) and noninvasive manner and included total body fat and fat free mass.

6.8. Elevated plus maze test

The Elevated Plus Maze (EPM) for mice consisted of intersecting perpendicular open arms (60 × 5 cm) and enclosed arms (60 × 5 cm) with 20 cm high walls. The maze was raised to a height of 50 cm above the floor level in a dimly lit room (20 Lux) and a video camera was suspended above the maze to record the movements for analysis. Each mouse was placed at the center of the platform, its head facing an open arm. The animals were tested individually and only once for 5 min. The maze was cleaned after each trial so as to remove any residue or odors. The following measurements were automatically taken and analyzed using a video-tracking software (Ethovision XT, Noldus, The Netherlands): the number of entries into the open or closed arms, the time spent in each arm, and the total distance moved in the EPM.

6.9. Forced swim test

Mice were individually forced to swim in an open cylindrical glass container (diameter 10 cm, height 25 cm), containing 10 cm of water at 25 ± 1 °C, for 6 min. The water was changed before the introduction of each animal. Mouse behavior was video-recorded by a video-camera placed in front of the glass cylinders. Activity was measured from the video recordings using video tracking software (Ethovision XT, Noldus, The Netherlands). Activity was scored using the mobility threshold settings within the Ethovision software by measuring the percentage change in area of the tracked object from one 0.08 s

time bin to the next. Activity was defined as either immobile (for changes in area between 0 and 10%) or strong mobile (for changes in area between 60 and 100%) during the last 4 min of the test.

6.10. Glycerol assay during cold and β3-AR challenge

To evaluate the acute thermogenic responses to cold, mice were moved to a fully environmentally controlled environment where the thermostat was set at 4 °C. For the selective β3 adrenergic receptor agonist challenge, CL-316243 (Sigma—Aldrich, St. Louis, MO) dissolved in sterile saline was administered i. p. at 1 mg/kg. For both procedures, mice were sampled 3 h after either the exposure to cold or the CL-316243 injection.

Glycerol was measured in mouse plasma samples using the Glycerol Assay Kit (MAK117, Sigma—Aldrich, St. Louis, MO) following the procedure recommended by the manufacturer. Glycerol standards were diluted with water to get final concentrations of 1.0, 0.6, 0.3, and 0 mM. Plasma samples were diluted with water, using a dilution factor of 4. The colorimetric assay was conducted in a 96-well plate and absorbance was measured using a plate reader (BioTek) at 570 nm. Using the glycerol standards, a standard curve was plotted and the slope was determined using linear regression. The measured absorbance values of the sample were first multiplied by the dilution factor, and then plasma glycerol concentrations were calculated using the measured absorbance of the sample divided by the slope of the standard curve.

7. INSULIN AND NE ELISA

Plasma insulin levels was measured using Mouse Ultrasensitive Insulin ELISA (ALPCO), and tissue NE was measured using the Noradrenaline (Norepinephrine) High Sensitive ELISA Assay kit from Eagle Biosciences (SKU: EA633/96) according to manufacturer's instructions.

7.1. Western blot

Western blot analysis of brain lysates was performed as previously described in detail [13], using anti-VGF C-terminal (1:2000, rabbit polyclonal) [27] or anti-β-actin (1:3000, # MAB1501, Millipore, Billerica, Massachusetts) antibodies. Membranes were washed in PBST, incubated with a secondary horseradish peroxidase-labelled donkey anti-rabbit or donkey anti-mouse antibody (1:6000, # NA934 and # NA931, GE Healthcare, Piscataway, New Jersey), washed in PBST, and incubated with ECL detection reagents (Millipore, Billerica, MA). Densitometric analysis was performed using NIH ImageJ software, and protein levels were normalized to β-actin.

Protein was extracted from frozen BAT in RIPA buffer (50 mm Tris—HCl, 150 mm NaCl, 1 mm EDTA, 0.5% Triton X-100, 1% sodium deoxycholate, 0.3% SDS, 0.1 mm PMSF, 0.2 mm 1, 10-phenoanthroline monohydrate, Phosphatase Inhibitor Cocktail A (Sigma—Aldrich, St. Louis, MO), Protease Inhibitor Cocktail (Sigma—Aldrich), and Phosphatase Inhibitor Cocktail 2 (Sigma—Aldrich, St. Louis, MO) by homogenization in Precellys CK28 Lysing Kit (Bertin, Catalog # 10,144—494) using a Minilys homogenizer (Bertin, Catalog #P000673-MLYS0-A). Homogenates were centrifuged for 30 min at 21000 g at 4 °C, with the supernatant collected and transferred to a new tube. The supernatant was centrifuged again at 21,000 g at 4 °C for 10 min, and the resulting supernatant was collected. Protein concentration for each sample was determined using the Pierce BCA Protein Assay Kit (Thermo Fisher Scientific, Waltham, MA). Equal amounts of protein were loaded into a 4—20% Bio-Rad Mini-Protean TGX Precast gels (Bio-Rad, Hercules, CA). Protein was transferred to a nitrocellulose membrane (Bio-Rad, Hercules, CA) using a Bio-Rad Trans-Blot Turbo Transfer System machine. Membranes were incubated in Revert Total Protein Stain (LiCor, #926—11011) and imaged on LiCor Imaging System. Transferred membranes were blocked with 5% Non-Fat dry milk (Cell-Signaling, Danvers, MA) in 1× TBST buffer (10 mm Tris-Base (Sigma—Aldrich, St. Louis, MO), 0.2 m NaCl (Macron Chemicals), 0.1% Tween-20 (Sigma—Aldrich, St. Louis, MO)), with a pH 7.4. Proteins were probed overnight with Anti-TH (Ab152 Rabbit Anti-Tyrosine Hydroxylase, Millipore Sigma, 1:1000 dilution in 2.5% Non-Fat milk in 1× TBST buffer). Reactivity was imaged using LiCor Imaging System (LI-COR Biosciences, Lincoln, NE), and immunoreactivity was quantified using LiCor Imaging software.

8. IMMUNOHISTOCHEMISTRY IN FROZEN TISSUES

Tissue from wild-type or ΔTLQP-21 mutant animals was harvested and fixed overnight in 4% PFA/PBS at 4 °C. The tissue was then dehydrated by storage in 30% (wt/vol) sucrose for a minimum of two days. Adrenal and brain tissue was embedded in OCT (optimal cutting temperature) compound using dry ice-cooled ethanol and cryosectioned (−20 °C) at a thickness of 20 μm mounted directly to charged slides (Fisherbrand Superfrost Plus). Slides containing collected cryosections were stored at −80 °C for later use. Collected adrenal sections were probed with antibodies for TLQP-21 (rabbit anti-TLQP-21, 1:100 [20]), Tyrosine Hydroxylase (sheep polyclonal TH, 1:100, Millipore Sigma, Burlington, MA), or NeuN (guinea pig anti-NeuN, 1:1000, Millipore Sigma, Burlington, MA) overnight at 4 °C in a humidified chamber. Nuclei were stained with Dapi (Biotium,Fremont, CA, cat. number 40043). The sections were the labeled with Alexa Flour-conjugated secondary antibodies (donkey anti-rabbit 488, donkey anti-sheep 647, donkey anti-guinea pig 488, donkey anti-rabbit 647, 1:500; Jackson ImmunoResearch Laboratories, West Grove, PA), counterstained with DAPI, and coverslips mounted using ProLong Gold mounting media (Invitrogen, Waltham, MA). Pseudocolor for NeuN and TLQP-21 were applied for the brain sections.

8.1. Morphological analysis of formalin-fixed paraffin-embedded (FFPE) adipose fat pads

Immediately after removal, tissue pieces representing BAT, scWAT and pWAT were fixed in 4% paraformaldehyde in 0.1 M phosphate buffer (pH 7.4) by overnight immersion at 4 °C. The samples were then dehydrated, cleared, and embedded in paraffin. Serial sections, from 3 different levels (100 μm apart), were respectively H&E-stained to assess their morphology and immunostained for UCP1 and TH. Immunostaining was performed as follows: 3-μm-thick sections were dewaxed, incubated with rabbit anti-UCP1 (1:500 v/v; ab10983, Abcam, Cambridge, UK) or sheep anti-TH (1:400 v/v; AB1542 Merck, Darmstadt, Germany) according to the avidin-biotin complex. Briefly: 1) endogenous peroxidase blocking with 3% hydrogen peroxide in methanol; 2) normal serum blocking (1:75) for 20 min to reduce nonspecific background; 3) incubation with primary antibodies at 4 °C; 4) secondary antibodies specific for rabbit or sheep, IgG biotin conjugated (1:200; Vector Labs, Burlingame, CA, USA); 5) ABC kit (Vector Labs, Burlingame, CA); and 6) enzymatic reaction to reveal peroxidase with Sigma Fast 3,3′-diaminobenzidine (Merck KGaA, Darmstadt, Germany) used as substrate. Finally, sections were counterstained and mounted in Eukitt (Fluka, Deisenhofen, Germany). For evaluation of TH-immunoreactive fiber density we collected random pictures using 100× oil immersion objective to reach 100 adipocytes for each animal ($n = 4$) of the two groups. We then counted the total number of TH-IR fibers. All observations were

performed with a Nikon Eclipse 80i light microscope (Nikon, Tokyo, Japan) equipped with a CCD camera. Brightness and contrast of the final images were adjusted using the Photoshop CS3 software (Adobe Systems; Mountain View, CA, USA).

8.2. qPCR

Total RNA was isolated from frozen tissue following the protocol listed in the RNeasy Lipid Tissue Mini Kit by Qiagen (Hilden, German, Catalog # 74,804). cDNA synthesis from RNA was completed using 5× iScript RT Supermix (Bio-Rad, Hercules, CA, Catalog #L001404 B) according to the manufacturer's protocol. Individual cDNA samples were run in duplicate using iTaq Universal SYBR Green Supermix (Bio-Rad, Hercules, CA, Catalog #L001752 B), with a final volume in each well equal to 15uL. A CFX Connect Real-Time System (Bio-Rad, Hercules, CA) thermal cycler and optic monitor was used. Gene expression data was normalized to the geometric mean of the best housekeeping gene, GAPDH, as determined by the program RefFinder [64]. Data was analyzed using the $\Delta\Delta C_t$ method and further normalized to the control group's mean. Primers are listed in Supplementary Table 5.

8.3. Statistical analysis

Statistical significance was determined by one or two way ANOVA or ANOVA for repeated measures with Tukey's post hoc test, with Student's t-test or with the non-parametric Mann—Whitney U test where appropriate. Statistica (TIBCO Software Inc., Palo Alto, CA) was used for analyses.

FUNDING

Supported by NIH/NIDDK R01DK117504 (A B and S.R.S.), NIH/NIDDK R56DK118150 (A.B.), NIH/NIDDK R01DK102496 (A.B.), Institute for Diabetes, Obesity and Metabolism University of Minnesota, 2022 Pilot and Feasibility Program (A.B.).

DECLARATION OF COMPETING INTEREST

The authors declare that they have no known competing financial interests or personal relationships that could have appeared to influence the work reported in this paper.

DATA AVAILABILITY

Data will be made available on request.

ACKNOWLEDGEMENT

Kohinoor Khan and Vinayak Ghosh are acknowledged for help with the study execution and figure preparation respectively.

APPENDIX A. SUPPLEMENTARY DATA

Supplementary data to this article can be found online at https://doi.org/10.1016/j.molmet.2023.101781.

REFERENCES

[1] Bartolomucci A, Possenti R, Mahata SK, Fischer-Colbrie R, Loh YP, Salton SRJ. The extended granin family: structure, function, and biomedical implications. Endocr Rev 2011;32(6):755—97. https://doi.org/10.1210/er.2010-0027.

[2] Sandoval DA, D'Alessio DA. Physiology of proglucagon peptides: role of glucagon and GLP-1 in health and disease. Physiol Rev 2015;95(2):513—48. https://doi.org/10.1152/physrev.00013.2014.

[3] Harno E, Gali Ramamoorthy T, Coll AP, White A. POMC: the physiological power of hormone processing. Physiol Rev 2018;98(4):2381—430. https://doi.org/10.1152/physrev.00024.2017.

[4] Kojima M, Matsui K, Mizui T. BDNF pro-peptide: physiological mechanisms and implications for depression. Cell Tissue Res 2019;377(1):73—9. https://doi.org/10.1007/s00441-019-03034-6.

[5] Sahu BS, Manna PT, Edgar JR, Antrobus R, Mahata SK, Bartolomucci A, et al. Role of clathrin in dense core vesicle biogenesis. Mol Biol Cell 2017;28(20). https://doi.org/10.1091/mbc.E16-10-0742.

[6] Stephens SB, Edwards RJ, Sadahiro M, Lin W-J, Jiang C, Salton SR, et al. The prohormone VGF regulates β cell function via insulin secretory granule biogenesis. Cell Rep 2017;20(10):2480—9. https://doi.org/10.1016/j.celrep.2017.08.050.

[7] Yaswen L, Diehl N, Brennan MB, Hochgeschwender U. Obesity in the mouse model of pro-opiomelanocortin deficiency responds to peripheral melanocortin. Nat Med 1999;5(9):1066—70. https://doi.org/10.1038/12506.

[8] Mountjoy KG, Caron A, Hubbard K, Shome A, Grey AC, Sun B, et al. Desacetyl-α-melanocyte stimulating hormone and α-melanocyte stimulating hormone are required to regulate energy balance. Mol Metabol 2018;9:207—16. https://doi.org/10.1016/j.molmet.2017.11.008.

[9] Zimmer AM, Pan YK, Chandrapalan T, Kwong RWM, Perry SF. Loss-of-function approaches in comparative physiology: is there a future for knockdown experiments in the era of genome editing? J Exp Biol 2019;222(Pt 7):jeb175737. https://doi.org/10.1242/jeb.175737.

[10] Trani E, Ciotti T, Rinaldi AM, Canu N, Ferri GL, Levi A, et al. Tissue-specific processing of the neuroendocrine protein VGF. J Neurochem 1995;65(6):2441—9. https://doi.org/10.1046/j.1471-4159.1995.65062441.x.

[11] Hahm S, Mizuno TM, Wu TJ, Wisor JP, Priest CA, Kozak CA, et al. Targeted deletion of the Vgf gene indicates that the encoded secretory peptide precursor plays a novel role in the regulation of energy balance. Neuron 1999;23(3):537—48. https://doi.org/10.1016/S0896-6273(00)80806-5.

[12] Watson E, Hahm S, Mizuno TM, Windsor J, Montgomery C, Scherer PE, et al. VGF ablation blocks the development of hyperinsulinemia and hyperglycemia in several mouse models of obesity. Endocrinology 2005;146(12):5151—63. https://doi.org/10.1210/en.2005-0588.

[13] Jiang C, Lin WJ, Sadahiro M, Labonté B, Menard C, Pfau ML, et al. VGF function in depression and antidepressant efficacy. Mol Psychiatr 2018;23(7):1632—42. https://doi.org/10.1038/mp.2017.233.

[14] Jiang C, Lin WJ, Labonté B, Tamminga CA, Turecki G, Nestler EJ, et al. VGF and its C-terminal peptide TLQP-62 in ventromedial prefrontal cortex regulate depression-related behaviors and the response to ketamine. Neuropsychopharmacology 2019;44(5):971—81. https://doi.org/10.1038/s41386-018-0277-4.

[15] Sadahiro M, Erickson C, Lin WJ, Shin AC, Razzoli M, Jiang C, et al. Role of VGF-derived carboxy-terminal peptides in energy balance and reproduction: analysis of "humanized" knockin mice expressing full-length or truncated VGF. Endocrinology 2015;156(5):1724—38. https://doi.org/10.1210/en.2014-1826.

[16] Bartolomucci A, La Corte G, Possenti R, Locatelli V, Rigamonti AE, Torsello A, et al. TLQP-21, a VGF-derived peptide, increases energy expenditure and prevents the early phase of diet-induced obesity. Proc Natl Acad Sci U S A 2006;103(39):14584—9. https://doi.org/10.1073/pnas.0606102103.

[17] Sahu BS, Nguyen ME, Rodriguez P, Pallais JP, Ghosh V, Razzoli M, et al. The molecular identity of the TLQP-21 peptide receptor. Cell Mol Life Sci 2021;78(23):7133—44. https://doi.org/10.1007/S00018-021-03944-1/FIGURES/3.

[18] Hannedouche S, Beck V, Leighton-Davies J, Beibel M, Roma G, Oakeley EJ, et al. Identification of the C3a receptor (C3AR1) as the target of the VGF-

derived peptide TLQP-21 in rodent cells. J Biol Chem 2013;288(38):27434–43. https://doi.org/10.1074/jbc.M113.497214.

[19] Cero C, Vostrikov VV, Verardi R, Severini C, Gopinath T, Braun PD, et al. The TLQP-21 peptide activates the G-protein-coupled receptor C3aR1 via a folding-upon-binding mechanism. Structure (London, England : 1993 2014;22(12):1744–53. https://doi.org/10.1016/j.str.2014.10.001.

[20] Possenti R, Muccioli G, Petrocchi P, Cero C, Cabassi A, Vulchanova L, et al. Characterization of a novel peripheral pro-lipolytic mechanism in mice: role of VGF-derived peptide TLQP-21. Biochem J 2012;441(1):511–22. https://doi.org/10.1042/BJ20111165.

[21] Fairbanks CA, Peterson CD, Speltz RH, Riedl MS, Kitto KF, Dykstra JA, et al. The VGF-derived peptide TLQP-21 contributes to inflammatory and nerve injury-induced hypersensitivity. Pain 2014;155(7):1229–37. https://doi.org/10.1016/j.pain.2014.03.012.

[22] D'Amato F, Noli B, Brancia C, Cocco C, Flore G, Collu M, et al. Differential distribution of VGF-derived peptides in the adrenal medulla and evidence for their selective modulation. J Endocrinol 2008;197(2):359–69. https://doi.org/10.1677/JOE-07-0346.

[23] Sahu BSBS, Rodriguez P, Nguyen MEME, Han R, Cero C, Razzoli M, et al. Peptide/receptor Co-evolution explains the lipolytic function of the neuropeptide TLQP-21. Cell Rep 2019;28(10):2567–80. https://doi.org/10.1016/j.celrep.2019.07.101. e6.

[24] Guo Z, Sahu BS, He R, Finan B, Cero C, Verardi R, et al. Clearance kinetics of the VGF-derived neuropeptide TLQP-21. Neuropeptides 2018;71:97–103. https://doi.org/10.1016/j.npep.2018.06.003.

[25] Duckert P, Brunak S, Blom N. Prediction of proprotein convertase cleavage sites. Protein Eng Des Sel: PEDS 2004;17(1):107–12. https://doi.org/10.1093/protein/gzh013.

[26] Jiang C, Lin W-J, Sadahiro M, Shin AC, Buettner C, Salton SR. Embryonic ablation of neuronal VGF increases energy expenditure and reduces body weight. Neuropeptides 2017;64:75–83. https://doi.org/10.1016/j.npep.2016.12.005.

[27] Lin W-J, Jiang C, Sadahiro M, Bozdagi O, Vulchanova L, Alberini CM, et al. VGF and its C-terminal peptide TLQP-62 regulate memory formation in Hippocampus via a BDNF-TrkB-dependent mechanism. J Neurosci : The Official Journal of the Society for Neuroscience 2015;35(28):10343–56. https://doi.org/10.1523/JNEUROSCI.0584-15.2015.

[28] Jedrychowski MP, Wrann CD, Paulo JA, Gerber KK, Szpyt J, Robinson MM, et al. Detection and quantitation of circulating human irisin by tandem mass spectrometry. Cell Metabol 2015;22(4):734–40. https://doi.org/10.1016/j.cmet.2015.08.001.

[29] Bartolomucci A, Pasinetti GM, Salton SRJ. Granins as disease-biomarkers: translational potential for psychiatric and neurological disorders. Neuroscience 2010;170(1):289–97. https://doi.org/10.1016/j.neuroscience.2010.06.057.

[30] Doolen S, Cook J, Riedl M, Kitto K, Kohsaka S, Honda CN, et al. Complement 3a receptor in dorsal horn microglia mediates pronociceptive neuropeptide signaling. Glia 2017;65(12):1976–89. https://doi.org/10.1002/glia.23208.

[31] Hunsberger JG, Newton SS, Bennett AH, Duman CH, Russell DS, Salton SR, et al. Antidepressant actions of the exercise-regulated gene VGF. Nat Med 2007;13(12):1476–82. https://doi.org/10.1038/nm1669.

[32] Bozdagi O, Rich E, Tronel S, Sadahiro M, Patterson K, Shapiro ML, et al. The neurotrophin-inducible gene Vgf regulates hippocampal function and behavior through a brain-derived neurotrophic factor-dependent mechanism. J Neurosci 2008;28(39):9857–69. https://doi.org/10.1523/JNEUROSCI.3145-08.2008.

[33] Cero C, Razzoli M, Han R, Sahu BS, Patricelli J, Guo Z, et al. The neuropeptide TLQP-21 opposes obesity via C3aR1-mediated enhancement of adrenergic-induced lipolysis. Mol Metabol 2017;6(1):148–58. https://doi.org/10.1016/j.molmet.2016.10.005.

[34] Jethwa PH, Warner A, Nilaweera KN, Brameld JM, Keyte JW, Carter WG, et al. VGF-derived peptide, TLQP-21, regulates food intake and body weight in Siberian hamsters. Endocrinology 2007;148(8):4044–55. https://doi.org/10.1210/en.2007-0038.

[35] Mamane Y, Chung Chan C, Lavallee G, Morin N, Xu L-J, Huang J, et al. The C3a anaphylatoxin receptor is a key mediator of insulin resistance and functions by modulating adipose tissue macrophage infiltration and activation. Diabetes 2009;58(9):2006–17. https://doi.org/10.2337/db09-0323.

[36] Stephens SB, Schisler JC, Hohmeier HE, An J, Sun AY, Pitt GS, et al. A VGF-derived peptide attenuates development of type 2 diabetes via enhancement of islet β-cell survival and function. Cell Metabol 2012;16(1):33–43. https://doi.org/10.1016/j.cmet.2012.05.011.

[37] Petrocchi-Passeri P, Cero C, Cutarelli A, Frank C, Severini C, Bartolomucci A, et al. The VGF-derived peptide TLQP-62 modulates insulin secretion and glucose homeostasis. J Mol Endocrinol 2015;54(3):227–39. https://doi.org/10.1530/JME-14-0313.

[38] Razzoli M, Bartolomucci A. The dichotomous effect of chronic stress on obesity. Trends Endocrinol Metabol 2016;27(7). https://doi.org/10.1016/j.tem.2016.04.007.

[39] Speakman JR, Król E, Johnson MS. The functional significance of individual variation in basal metabolic rate. Physiol Biochem Zool p 2004;77:900–15.

[40] Reitman ML. Of mice and men — environmental temperature, body temperature, and treatment of obesity. FEBS (Fed Eur Biochem Soc) Lett 2018;592(12):2098–107. https://doi.org/10.1002/1873-3468.13070.

[41] Succu S, Mascia MS, Melis T, Sanna F, Melis MR, Possenti R, et al. Pro-VGF-derived peptides induce penile erection in male rats: involvement of paraventricular nitric oxide. Neuropharmacology 2005;49(7):1017–25. https://doi.org/10.1016/j.neuropharm.2005.05.015.

[42] Pinilla L, Pineda R, Gaytán F, Romero M, García-Galiano D, Sánchez-Garrido MA, et al. Characterization of the reproductive effects of the anorexigenic VGF-derived peptide TLQP-21: in vivo and in vitro studies in male rats. Am J Physiol Endocrinol Metab 2011;300(5):E837–47. https://doi.org/10.1152/ajpendo.00598.2010.

[43] Aguilar E, Pineda R, Gaytán F, Sánchez-Garrido MA, Romero M, Romero-Ruiz A, et al. Characterization of the reproductive effects of the Vgf-derived peptide TLQP-21 in female rats: in vivo and in vitro studies. Neuroendocrinology 2013;98(1):38–50. https://doi.org/10.1159/000350323.

[44] Lewis JE, Brameld JM, Hill P, Cocco C, Noli B, Ferri G-L, et al. Hypothalamic over-expression of VGF in the Siberian hamster increases energy expenditure and reduces body weight gain. PLoS One 2017;12(2):e0172724–e0172724. https://doi.org/10.1371/journal.pone.0172724.

[45] Speakman JR. Measuring energy metabolism in the mouse - theoretical, practical, and analytical considerations. Frontiers in Physiology 4 MAR 2013. https://doi.org/10.3389/fphys.2013.00034.

[46] Tschöp MH, Speakman JR, Arch JRS, Auwerx J, Brüning JC, Chan L, et al. A guide to analysis of mouse energy metabolism. Nat Methods 2012;9(1):57–63. https://doi.org/10.1038/nmeth.1806.

[47] Careau V, Halsey LG, Pontzer H, Ainslie PN, Andersen LF, Anderson LJ, et al. Energy compensation and adiposity in humans. Curr Biol: CB 2021;31(20):4659–66. https://doi.org/10.1016/j.cub.2021.08.016. e2.

[48] Hall KD. Energy compensation and metabolic adaptation: "The Biggest Loser" study reinterpreted. Obesity (Silver Spring, Md 2022;30(1):11–3. https://doi.org/10.1002/oby.23308.

[49] O'Neal TJ, Friend DM, Guo J, Hall KD, Kravitz AV. Increases in physical activity result in diminishing increments in daily energy expenditure in mice. Curr Biol: CB (Curr Biol) 2017;27(3):423–30. https://doi.org/10.1016/j.cub.2016.12.009.

[50] Chouchani ET, Kazak L, Spiegelman BM. New advances in adaptive thermogenesis: UCP1 and beyond. Cell Metabol 2019;29(1):27–37. https://doi.org/10.1016/j.cmet.2018.11.002.

[51] Bachman ES, Dhillon H, Zhang C-Y, Cinti S, Bianco AC, Kobilka BK, et al. Beta AR signaling required for diet-induced thermogenesis and obesity resistance. Science 2002;297(5582):843–5. https://doi.org/10.1126/science.1073160.

[52] Cannon B, Nedergaard J. Brown adipose tissue: function and physiological significance. Physiol Rev 2004;84(1):277—359. https://doi.org/10.1152/physrev.00015.2003.

[53] Chen Y, Ikeda K, Yoneshiro T, Scaramozza A, Tajima K, Wang Q, et al. Thermal stress induces glycolytic beige fat formation via a myogenic state. Nature 2019;565(7738):180—5. https://doi.org/10.1038/s41586-018-0801-z.

[54] Razzoli M, Frontini A, Gurney A, Mondini E, Cubuk C, Katz LS, et al. Stress-induced activation of brown adipose tissue prevents obesity in conditions of low adaptive thermogenesis. Mol Metabol 2016;5(1):19—33. https://doi.org/10.1016/j.molmet.2015.10.005.

[55] Zeng X, Ye M, Resch JM, Jedrychowski MP, Hu B, Lowell BB, et al. Innervation of thermogenic adipose tissue via a calsyntenin 3β-S100b axis. Nature 2019;569(7755):229—35. https://doi.org/10.1038/s41586-019-1156-9.

[56] Yoneshiro T, Wang Q, Tajima K, Matsushita M, Maki H, Igarashi K, et al. BCAA catabolism in brown fat controls energy homeostasis through SLC25A44. Nature 2019;572(7771):614—9. https://doi.org/10.1038/s41586-019-1503-x.

[57] Sveidahl Johansen O, Ma T, Hansen JB, Markussen LK, Schreiber R, Reverte-Salisa L, et al. Lipolysis drives expression of the constitutively active receptor GPR3 to induce adipose thermogenesis. Cell 2021;184(13):3502—18. https://doi.org/10.1016/j.cell.2021.04.037. e33.

[58] Kazak L, Chouchani ET, Jedrychowski MP, Erickson BK, Shinoda K, Cohen P, et al. A creatine-driven substrate cycle enhances energy expenditure and thermogenesis in beige fat. Cell 2015;163(3):643—55. https://doi.org/10.1016/j.cell.2015.09.035.

[59] Bal NC, Maurya SK, Sopariwala DH, Sahoo SK, Gupta SC, Shaikh SA, et al. Sarcolipin is a newly identified regulator of muscle-based thermogenesis in mammals. Nat Med 2012;18(10):1575—9. https://doi.org/10.1038/nm.2897.

[60] Alquier T, Poitout V. Considerations and guidelines for mouse metabolic phenotyping in diabetes research. Diabetologia 2018;61(3):526—38. https://doi.org/10.1007/s00125-017-4495-9.

[61] Fargali S, Garcia AL, Sadahiro M, Jiang C, Janssen WG, Lin W-J, et al. The granin VGF promotes genesis of secretory vesicles, and regulates circulating catecholamine levels and blood pressure. FASEB (Fed Am Soc Exp Biol) J : Official Publication of the Federation of American Societies for Experimental Biology 2014;28(5):2120—33. https://doi.org/10.1096/fj.13-239509.

[62] MacLean B, Tomazela DM, Abbatiello SE, Zhang S, Whiteaker JR, Paulovich AG, et al. Effect of collision energy optimization on the measurement of peptides by selected reaction monitoring (SRM) mass spectrometry. Anal Chem 2010;82(24):10116—24. https://doi.org/10.1021/ac102179j.

[63] Palanza PL, Howdeshell KL, Parmigiani S, vom Saal FS. Exposure to a low dose of bisphenol A during fetal life or in adulthood alters maternal behavior in mice. Environ Health Perspect 2002;110(Suppl 3):415—22. https://doi.org/10.1289/ehp.02110s3415. Suppl 3.

[64] Xie F, Xiao P, Chen D, Xu L, Zhang B. miRDeepFinder: a miRNA analysis tool for deep sequencing of plant small RNAs. Plant Mol Biol 2012. https://doi.org/10.1007/s11103-012-9885-2.

